J. Biomedical Science and Engineering, 2011, 4, 755-761 **JBiSE**
doi:10.4236/jbise.2011.412093 Published Online December 2011 (http://www.SciRP.org/journal/jbise/).

Imaging of arterial plaque by quadrature swept-source optical coherence tomography with signal to noise ratio enhancements

Youxin Mao*, Costel Flueraru, Shoude Chang

Institute for Microstructural Sciences, National Research Council Canada, Ottawa, Canada.
Email: *linda.mao@nrc-cnrc.gc.ca

Received 18 August 2011; revised 5 October 2011; accepted 11 November 2011.

ABSTRACT

Arterial plaque from a myocardial infarction-prone Watanabe heritable hyperlipidemic (WHHLMI) rabbit is visualized and characterized using a signal to noise ratio enhanced swept-source optical coherence tomography system with a quadrature interferometer (QSS-OCT). A semiconductor optical amplifier is used in the sample arm to amplify the weak signal scattered from arterial plague. Signal to noise ratio improvement are demonstrated in our QSS-OCT system. This finding results into an increase of the penetration depth possible in OCT images, from 1 mm to 2 mm. Preliminary results show that vulnerable plaque with fibrous cap, macrophage accumulations and calcification in the arterial tissue are measurable with our QSS-OCT system.

Keywords: Optical Coherence Tomography; Arterial Plaque; Medical and Biological Imaging; Semiconductor Optical Amplifier

1. INTRODUCTION

The identification of unstable plaque is central in risk-stratifying patients for acute coronary events. Optical coherence tomography (OCT) [1] is a recently introduced imaging modality that has shown considerable promise for the identification of high-risk plaques. The advantages of OCT compared to ultrasound include its higher resolution, video speed acquisition rate, compactness and portability. When a small and inexpensive optical fiber probe as an optical catheter constitutes the sample arm, the system becomes suitable for intra-vascular probing [2]. Because OCT uses light, a variety of functional and spectroscopic techniques are available to expand its capabilities, including polarization, absorption, elastography, Doppler, and dispersion analysis.

An OCT system with higher signal-to-noise ratio (SNR) is essentially important for imaging turbid tissues, such as arterial plaques, because the backscattered signals from these types of samples are extremely weak. Swept-source OCT (SS-OCT) has received much attention in recent years not only because of its higher SNR at high imaging speeds but also for its imaging possibilities in the 1300 nm wavelength range, where the reduced light scattering by tissue enables OCT to collect signal from deeper into tissue compared to OCT imaging based on shorter source wavelengths. SS-OCT could also use the quadrature interferometer based on multi-port fiber couplers such as the 3 × 3 quadrature interferometer [3]. When measuring instantaneous complex signals with stable phase information by using a 3 × 3 quadrature interferometer one can suppress the complex conjugate artefact and therefore double the effective imaging depth [4,5]. The phase information of the complex interferometric signals can also be exploited to gain additonal information about the tissue, to enhance image contrast and to perform quantitative measurements. In addition, the Mach-Zehnder configuration of the presented interferometric setup (MZI) allows different options to distribute optical power between the reference and sample arms. An unbalanced input directs more optical power from the light source to the sample than that to the reference mirror [6] while the balanced detection is used to reduce the beat noise [7]. Both techniques play their parts in increasing SNR. However in the case of imaging turbid biomedical samples, the signal backscattered from tissue is much weaker than the reference signal so an attenuation of optical power in the reference arm is required in order to increase the SNR. The ability of OCT to image vascular plaque has been previously demonstrated [8-11]. However, OCT images of the arterial wall are limited to depths of ~1 mm even using the Fourier domain methods [2]. The limited imaging depth into the vascular wall is one of the most serious limitations for OCT to be used as a routine clinical intravascular imaging method. Further improvement of the SNR of OCT is needed in order to increase the imaging depth of OCT into tissue. Adding an optical amplifier in the path of the backscattered signal in the sample arm of an SS-OCT

system with a balanced Michelson interferometer [12] and a 2 × 2 MZI configuration [13,14] has been proposed. Modest amount improvement of signal to noise ratio or sensitivity had reported in their configurations. However, in our knowledge, no OCT image improvement in cardiology applications has been reported.

In this paper, we theoretically and experimentally demonstrate a SS-OCT system with a quadrature interferometer (QSS-OCT) using a semiconductor optical amplifier (SOA) for the amplification of the weak signal existent in the sample arm. Improvement of SNR is demonstrated. Lipid-rich plaque of a WHHLMI rabbit is visualized and characterized with this system. Preliminary results show that vulnerable plaque with fibrous cap, macrophage accumulations and calcification in the arterial tissue are measurable with our QSS-OCT system, which is also able to image features located as deep as 2 mm from the lumen surface.

2. METHODS AND MATERIALS

Figure 1 shows an experimental setup of our QSS-OCT system that uses a balanced 3 × 3 and 2 × 2 quadrature MZI and a SOA for weak sample signal amplification. The swept laser source (HSL2000-HL, Santac) used in the setup had a central wavelength of 1320 nm and a full scan wavelength range of 110 nm, was swept linearly in optical frequency with a linearity of 0.2%. The bandwidth of the source corresponds to an 8-μm OCT imaging resolution in the air. The average output power and coherence length of the swept source was 12 mW and 10 mm, respectively. A repetition scan rate of 20 kHz was used in our system and the related duty cycle was 68%. The light output from the swept laser source was launched first into the 2 × 2 coupler where 90% of the power was diverted toward the sample. The reference arm was arranged with a fiber collimator and a mirror. The light was directed to the sample through a lensed single mode fiber probe [15]. A galvanometer (Blue Hill Optical technologies) scanned the fiber probe along the sample surface up to 4 mm-long trip corresponding to an OCT image width of 900 pixels. The weak light back- scattered from the sample was fed into a SOA (Covega) whose gain can be adjusted by a variable attenuator connected after the SOA. The SOA had the same center wavelength and bandwidth as the swept source. The gain could be varied from 15 dB to 35 dB. The reference arm has been build so that it can match the optical distance of the sample arm without SOA and by adding an optical jumper with certain length it can match the optical distance of the sample arm with SOA. Both, the SOA and the added optical jumper (part of reference arm) could be removed allowing the system to be switched back to a regular QSS-OCT system without sample signal amplification. A polarization controller was inserted before the SOA for optimal amplification. The amplified signal was combined with the signal returning from the reference mirror through the 3 × 3 and 2 × 2 couplers, thus implementing a dual-channel balanced detection system with two complementary components of the complex interferometric signals which suppresses the complex conjugate artefact. Both balanced detectors (PDB150C, Thorlabs) used in this system had saturation powers of 5 mW. We selected a 3 dB bandwidth of 50 MHz to give sufficient imaging depth. The two detector outputs were

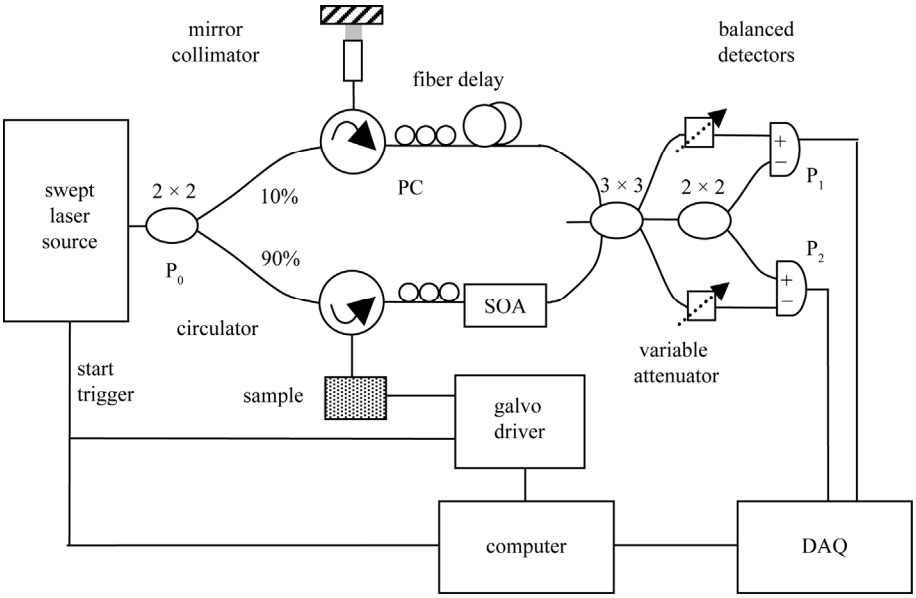

Figure 1. Experimental setup of our QSS-OCT system with a balanced 3 × 3 and 2 × 2 quadrature MZI and an SOA for the amplification of the signal back-scattered from the sample.

Copyright © 2011 SciRes.

digitized using a data acquisition card (DAQ) (Alazartech, Montreal) with 14-bit resolution and acquired signal at a sampling speed of 100 MS/s. The swept source generated a start trigger signal that was used to initiate the function generator for the galvo scanner and initiate the data acquisition process for each A-scan. Because the swept source was linearly swept with the wave-number k, A-scans data with resolved complex conjugate artifact were obtained by a direct inverse Fourier transformation (IFT) from the DAQ sampled data without performing an additional re-sampling step.

Watanabe heritable hyperlipidemic (WHHLMI) rabbit is a suitable animal model to study familial hypercholesterolemia and atherosclerosis. Arteries in these rabbits develop atheromatous plaques similar to those in humans [16]. **Figure 2(a)** shows a picture of a segment of the descending aorta together with the protected forward-view ball fiber probe collecting an OCT image in this work. The size of the OCT probe and the properties of the probing beam are important for OCT imaging. An optical fiber-lensed probe with a diameter as small as 0.5 mm is suitable for OCT imaging, especially for *in vivo* intravascular imaging. Based on interaction of near infrared light with different human tissues, the range of penetration depth is from 0.5 mm to 3 mm [17]. Working distance range of an ultra-small fiber-based lense [15] can be designed from 0.4 to 1.2 mm for matching the penetration depth of tissues tested. Depth of field can be in the range of 0.3 - 1.5 mm, which corresponds the spot size range of 15 - 35 μm at the 1300 nm wavelength, because the tradeoff between the depth of field and beam spot size for a Gaussian beam. For imaging arterial tissue, a fiber ball lens was designed and fabricated in house with a ball size of 0.3 mm, the working distance of 1.25 mm, depth of field of 1.0 mm, and $1/e^2$ spot diameter of 29 μm shown in the inset of **Figure 2(a)** as a forward—view probe. To form a side-view fiber probe, the output beam can be total internal reflected 90 - 100 degree by a 45 - 50 degree polished face on the fiber ball. As a sample, a needle delivered fiber catheter probe designed for the OCT intravascular imaging is shown in **Figure 2(b)**. The polished lens and the uncoated portion of the SMF are protected in a transparent inner catheter (OD 0.49 mm) shown in the inset of **Figure 2(b)**. The buffered portion of the fiber is attached to an outer flexible catheter (OD 1.4 mm) after a syringe, which is fastened onto a modified syringe piston (not shown here), while the transparent inner catheter is inserted into a 21 G (OD 0.81 mm) echogenic spinal needle (VWR, Mississauga, ON, Canada). After insertion into the tissue,

(a)

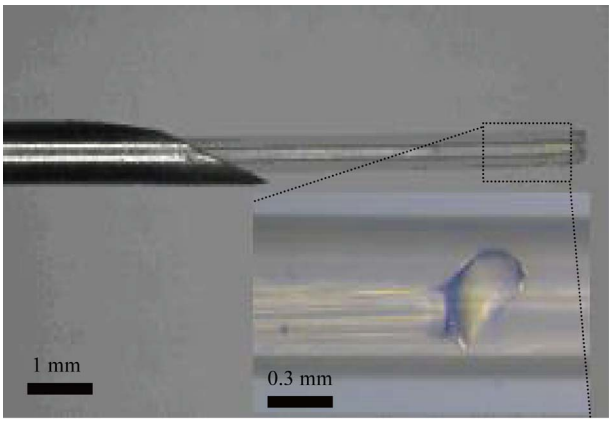

(b)

Figure 2. (a) An opened left descending coronary tissue from a Watanabe heritable hyperlipidemic (WHHLMI) rabbit being scanned with the forward ball lens fiber probe protected by a plastic tube. Inset: A scanning electron micrograph of the fiber ball lens with forward-view fabricated in our lab. (b) A needle tip of a side-view fibber ball lens probe as a sample of an OCT probe for *in vivo* intravascular imaging.

the needle can be drawn back a small distance to let the optical probe expose to the tissue as shown in **Figure 2(b)**. The probe is then scanned axially inside the tissue driven by a linear scanner, such that a two dimensional OCT image is formed.

3. SIGNAL TO NOISE RATIO ANALYSIS

To estimate SNR in our QSS-OCT system shown in **Figure 1(a)**, assuming that the signal in the sample arm is coming from a single layer reflector located at the depth of z_0, the two channel currents on the positive and negative photodiodes in each balanced detector when the SOA is inserted into the sample arm are given by [14, 18]:

$$I_{1\pm}(k_m,G)=\alpha\left[P_{r\pm}(k_m)+P_{s\pm}(k_m,G)+P_{SP\pm}(G)\pm 2\sqrt{P_{r\pm}(k_m)P_{s\pm}(k_m,G)}\cos(2k_m z_0+\phi)\right] \quad (1)$$

Copyright © 2011 SciRes.

$$I_{2\pm}(k_m,G)=\alpha\left[P_{r\pm}(k_m)+P_{s\pm}(k_m,G)+P_{SP\pm}(G)\pm 2\sqrt{P_{r\pm}(k_m)P_{s\pm}(k_m,G)}\cos(2k_m z_0+\phi+\Delta\phi)\right] \quad (2)$$

where, $\alpha=\eta e/(h\nu_0)$ is photodiode conversion factor, η is the quantum efficiency of the detector, e is the electronic charge, h is the Planck's constant, ν_0 is the mean frequency of the incident light, $P_r(k_m)$ is the optical signal power from the reference arm arriving at the photodiodes when wavenumber $k = k_m$, $P_s(k_m,G)$ is the amplified optical signal power from the sample arm at the photodiodes when wavenumber $k = k_m$, $P_{SP}(G)$ is the spontaneous emission power of the SOA recorded at the photodiodes, G is the gain of SOA, ϕ is an arbitrary phase shift, $\Delta\phi$ is the phase shift between the two output signals, m = 1, 2, $\cdots$, M, *where* M is the total sampling number of the axial pixels. Balanced detection subtracts each positive and negative current for each channel shown in **Eqs.1** and **2**, so that the common DC parts are subtracted and the opposite AC parts are multiplied. The complementary phase components of the signals can be calculated by **Eqs.8** and **9** in Ref. [4] for a complex discrete Fourier transform (DFT). Then, the maximum-squared signal power in our system with the dual-balanced quadrature detection is given as [18]:

$$\left\langle I(G)^2\right\rangle=(4D\alpha)^2 P_r P_s(G) \quad (3)$$

where the brackets denote the ensemble average, P_r is the optical power impinging on each photodiode reflected from the reference mirror. $P_s(G)$ is the amplified signal power incident on each photodiode backscattered from the sample. D is a multiplied factor coming from complex IFT, with D = 2 in our setup.

In this configuration there are three typical noise sources: thermal noise, shot noise and beat noise [19]. By extending the noise analysis of SS-OCT [18] with slightly mismatched balanced detection [20] to our QSS-OCT system with the SOA inserted into on the sample arm, the total noise power as a function of the SOA gain, G, is obtained:

$$\left\langle\sigma(G)^2\right\rangle=DB\left\{i_{th}^2+4e\alpha\left(P_r+P_{SP}(G)\right)+2\alpha^2\left[2\beta(2-\beta)RIN_b P_r P_{sp}(G)+(1-\beta)^2\left(RIN_r P_r^2+RIN_s P_{sp}(G)^2\right)\right]\right\} \quad (4)$$

where, B is the detector bandwidth, i_{th} is the thermal current of the detector, β is a balanced factor [21] with β = 1 representing a balanced system, $RIN_{r/s} = 2/\delta\nu_{r/s}$ is the relative intensity noise of source and SOA, $\delta\nu_r$ and $\delta\nu_s$ is their effective bandwidth, respectively. RIN_b is the relative cross-beat intensity noise from the reference light and the spontaneous emission power of the SOA, which can be estimated from the experimental results. The first and second terms in **Eq.4** are thermal noise and shot noise as commonly expressed. The third term represents the beat noise, which includes the cross-beat and self-beat noise of the two arms. If the losses and reflectivities of the reference and sample arms are defined as γ_r, R_r and γ_s, R_s, then the powers from the reference and sample arms impinging on the photodiodes can be described as $P_o\gamma_r AR_r$ and $P_o\gamma_s GR_s$, respectively, where A is the reference attenuation when the sample signal is not being amplified. If the loss from the SOA to the detector is defined as γ, the spontaneous emission power of the SOA impinging on the photodiodes can be written as γP_{sp}. The *SNR* of our QSS-OCT system with the SOA inserted for weak sample signal amplification is described as:

$$SNR(G)=\frac{16D\alpha^2 P_0^2\gamma_r A^2 R_r\gamma_s GR_s}{B\left\{i_{\det}^2+4e\alpha\left(P_0\gamma_r A^2 R_r+\gamma P_{sp}(G)\right)+2\alpha^2\left[2\beta(2-\beta)RIN_b P_0\gamma_r A^2 R_r\gamma P_{sp}(G)+(1-\beta)^2\left(RIN_r\left(P_0\gamma_r A^2 R_r\right)^2+RIN_s\gamma^2 P_{sp}(G)^2\right)\right]\right\}} \quad (5)$$

Figure 3 shows the calculated results for various noise powers (a) and SNR (b) versus SOA gain, G, when the QSS-OCT system contains a sample signal amplifier (right-side horizontal axis) and versus reference arm attenuation, A, when the QSS-OCT system without a sample signal amplifier (left-side horizontal axis). The calculations are based on the following assumptions: λ_0 = 1.32 μm, $\delta\lambda_r$ = 1 nm, P_0 = 12 mW, γ_r = –20 dB, γ_s = –10.5 dB, γ = –9 dB, R_r = 0 dB, R_s = –55 dB, B = 50 MHz, β = 0.99, i_{th} = 2 n A/sqrt (Hz), $\delta\lambda_s$ = 100 nm, $P_{sp} = P_{sp0}G$, $P_{sp0} = 10^{-3}$ mW.

From the theoretical analysis results shown in **Figure 3**, when the QSS-OCT system without the SOA, reference light power could be attenuated to reduce the reference power self-beat noise and to obtain the shot-noise limit. When the QSS-OCT system contains the SOA on the sample arm, the SNR can be increased as the gain of SOA increase although the system is no longer shotnoise

Copyright © 2011 SciRes.

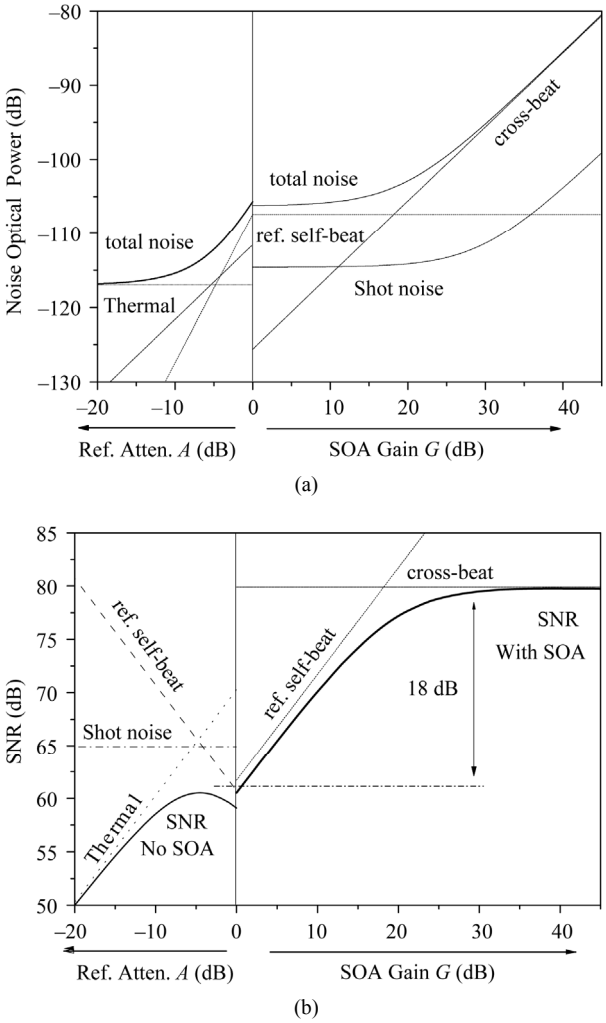

Figure 3. Theoretical analysis results of various noise powers (a) and SNR (b) versus SOA gain, *G*, when the QSS-OCT system contains a sample signal amplifier (right-side horizontal axis) and versus reference arm attenuation, A, when the QSS-OCT system without a sample signal amplifier (left-side horizontal axis).

limit. When the gain of sample arm SOA is low, < 15 dB, reference (ref.) self-beat noise dominates the cross-beat noise, the SNR linearly increases as the gain is increased because the ref. self-beat noise stays constant as the gain increases. Because the cross-beat noise from the reference power and the spontaneous power emission of the SOA increases as the gain increases, when $G > 15$ dB, the cross-beat noise raises to the level of the ref. self-beat noise, increase of SNR becomes slowly. As the gain continuously increases to $G > 30$ dB, SNR will saturate where the cross-beat noise becomes dominant. Increase of SNR up to 18 dB is calculated when the QSS-OCT system contains the optical amplifier in comparison with the system without the optical amplifier in the shot noise limit as shown in **Figure 3**.

4. RESULTS AND DISCUSSION

Figure 4(a) shows an *ex vivo* OCT image of a segment of aorta where the image was acquired using the QSS-OCT system with a 25 dB gain SOA inserted in sample arm. The axial and lateral dimensions of the image are 500 × 900 pixels respectively which correspond to an image size of 2 × 3 mm^2. The image size is calibrated using a 1 mm glass slice and assume refractive index of arterial is 1.3. In **Figure 4(a)**, a clear raised lipid core with macrophage accumulation with un-uniform reflectance within its volume (black arrows) is shown. A thin fibrous cap, which strongly scatters light, covers the lipid core (white circle). The fibrous cap was defined as the minimum distance from the coronary artery lumen to the upper border of the lipid pool. A few calcified regions (white arrows) around the lipid core, characterized itself by low reflectance, are clearly discernable. The regions with uniform reflectance (grey arrows) correspond to bundles of smooth muscle cells, which can be viewed up to depths of 2 mm even beneath the calcified regions. The results obtained from images of WHHLMI coronaries acquired with our QSS-OCT, as the image shown in **Figure 4(a)**, agreed very well with the histological micrographs of these samples, shown in the **Figure 4** of ref. [16]. For comparison, an OCT image acquired at the same position on the sample after the SOA was extracted from the sample arm is shown in **Figure 4(b)**. Obviously, the image shown in **Figure 4(b)** does not provide a clear view of all the clinical aspects of the sample, especially in the regions located deeper than 1 mm. To further quantify the analysis, we selected three A-scan profiles which are illustrated in **Figures 4(c)-(e)**. These intensity profiles are shown as they were acquired with the QSS-OCT system when it had an SOA (black) inserted and without SOA inserted (grey). These three scans are located at the positions marked with dashed arrows in **Figures 4(a)** and **(b)**. By comparing the data recorded when the system had the SOA with the data recorded by the system without SOA, it can be observed that the signal values increase up to 25 dB while the levels of noise increase by only 10 dB, so that SNR of 15 dB is increased. Signals coming from structures located at depths of up to 2 mm can be observed in the data acquired with the system that has the SOA inserted. However, structures located at and deeper than 1 mm become difficult to distinguish when the SOA is removed. The increase in the image penetration depth when acquired by the QSS-OCT with the SOA inserted is also evident in **Figure 4(a)** from the ability to distinguish the calcification boundary. The identified features from **Figure 4(a)** can be quantified as follows: the size of macrophage accumulation core is 1.0 mm (lateral) by 0.79 mm (depth) with a 36 μm thickness the fibrous cap, while the sizes

Copyright © 2011 SciRes.

of the calcified regions are 0.6 mm by 0.4 mm (left side), 0.3 mm by 0.15 mm (right side).

To view changes of the clinical aspects of the plaque along the direction of blood flow, a series of the cross-section OCT images were taken from the positions along the blood flow. **Figure 5** shows six images of the coronary from the WHHLMI rabbit in 0.1 mm apart along the blood flow acquired utilizing the QSS-OCT system with a 25 dB gain SOA inserted in sample arm. Each image is in the same size as that shown in **Figure 4**. These images formed a three-dimensional (3D) view of the coronary of the WHHLMI rabbit. Size and density changes of the clinical aspects of the coronary along the blood flow were clearly distinguished from the 3D view. A lipid core (black arrows), several calcified regions (white arrows) with large size change in the 0.6 mm distance, and another lipid-rich area (grey arrows) beneath the calcified regions. This lipid-rich area becomes larger to a size of 1.5 × 1 mm^2 along the calcified regions shrink, while its fibrous cap (black diamond) remains

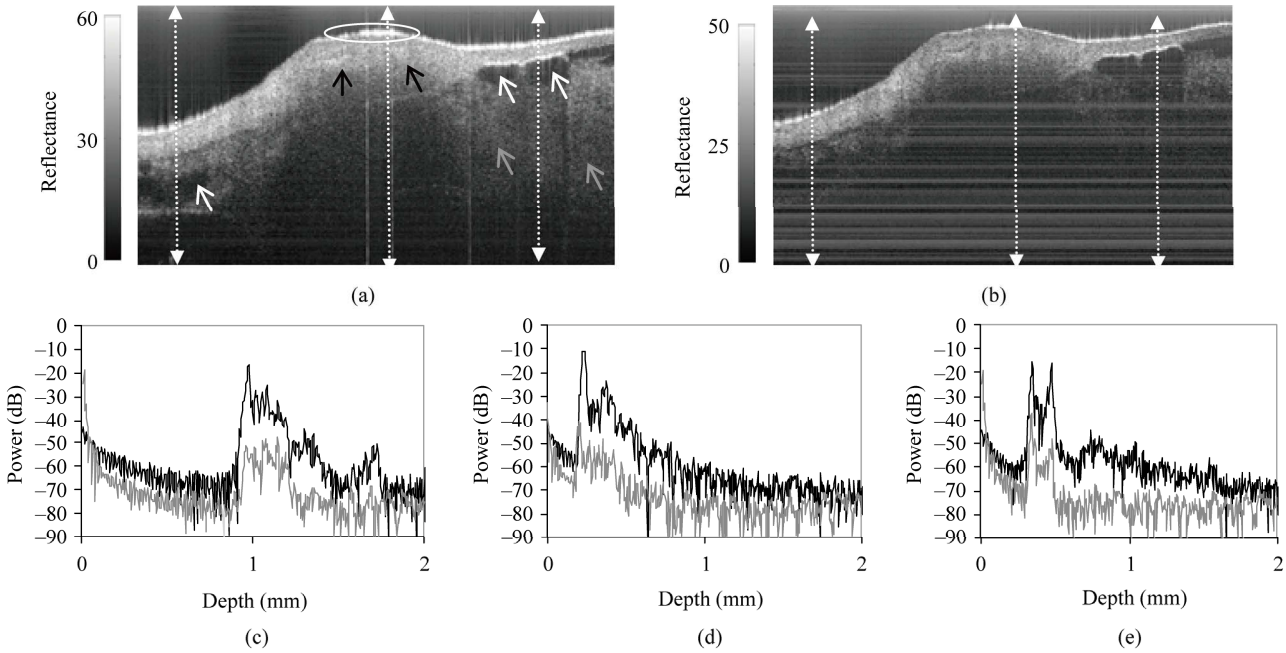

Figure 4. *Ex vivo* OCT images of a coronary from a WHHLMI rabbit acquired by the QSS-OCT system with the sample signal amplifier (a) and without (b). A-scan signals at the positions of the dashed arrow lines with pixels 100 (c), 500 (d), and 750 (e) acquired by the QSS-OCT system with the sample signal amplifier (black) and without SOA (grey).

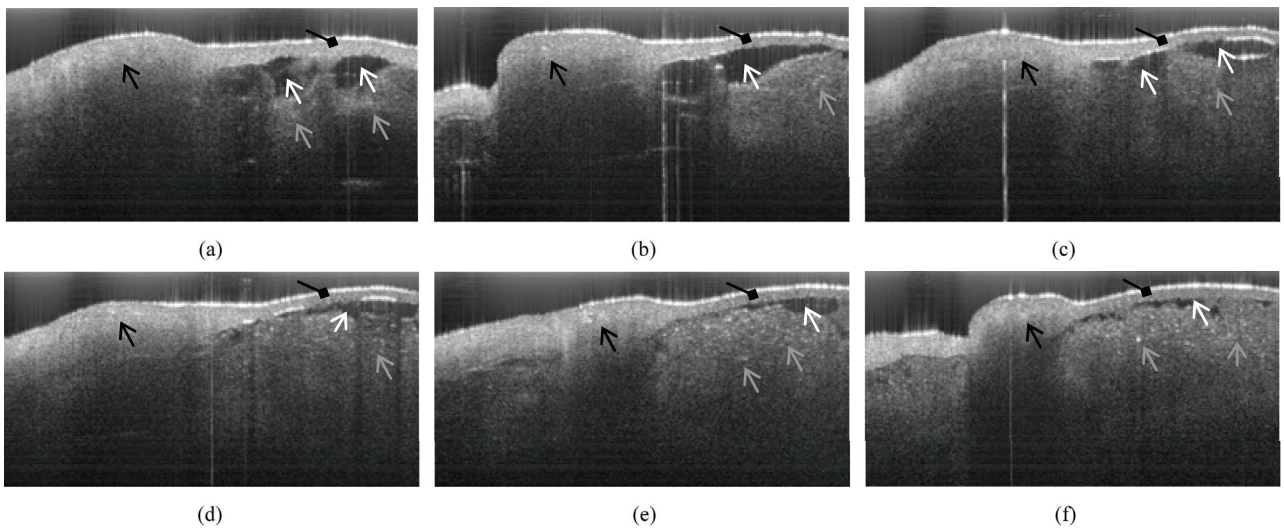

Figure 5. *Ex vivo* OCT images in another location of the coronary from the WHHLMI rabbit acquired by the QSS-OCT system with the sample signal amplifier. Each image is taken from the positions in 0.1 mm apart.

Copyright © 2011 SciRes.

around 0.25 mm.

5. CONCLUSION

High quality images of descending aorta harvested from WHHLMI rabbits are produced by using a quadrature swept-source OCT system containing a semiconductor optical amplifier in the sample arm. A significant increase in signal-to-noise ratio was obtained by inserting an SOA in the sample arm of the QSS-OCT system. The penetration depth of the QSS-OCT image was increased with the addition of sample signal amplification. Preliminary results show that vulnerable plaque with fibrous caps, macrophage accumulations and calcifications present in arterial tissue are measurable with our QSS-OCT system. Our new QSS-OCT system reported in this work could help in identify the locations of vulnerable coronary plaques, *in vivo*, and in monitoring, with a high degree of detail, the outcomes of coronary interventions.

6. ACKNOWLEDGMENTS

The authors are grateful to Dan P. Popescu, and Michael G. Sowa from Institute for Biodiagnostics, National Research Council Canada, for providing the coronary samples of WHHLMI rabbit.

REFERENCES

[1] Huang, D., Swanson, E.A., Lin, C.P., Schuman, J.S., Stinson, W.G., Chang, W., Hee, M.R., Flotte, T., Gregory, K., Puliafito, C.A. and Fujimoto, J.G. (1991) Optical coherence tomography. *Science*, **254**, 1178-1181. doi:10.1126/science.1957169

[2] Barils, P. and Schmitt, J. (2009) Current and future developments in intracoronary optical coherence tomography imaging. *EuroInterv*, **4**, 529-533. doi:10.4244/EIJV4I4A89

[3] Sarunic, M.V., Choma, M.A., Yang, C. and Izatt, J.A. (2005) Instantaneous complex conjugate resolved spectral domain and swept-source OCT using 3 × 3 fiber couplers. *Optics Express*, **13**, 957-967. doi:10.1364/OPEX.13.000957

[4] Mao, Y., Sherif, S., Flueraru, C. and Chang, S. (2008) 3 × 3 Mach-Zehnder interferometer with unbalanced differential detection for full range swept-source optical coherence tomography. *Applied Optics*, **47**, 2004-2010. doi:10.1364/AO.47.002004

[5] Flueraru, C., Kumazaki, H., Sherif, S., Chang, S. and Mao, Y. (2007) Quadrature Mach-Zehnder interferometer with application in optical coherence tomography. *Journal of Optics A*: *Pure and Applied Optics*, **9**, L5-L8. doi:10.1088/1464-4258/9/4/L01

[6] Rollins, A.M. and Izatt, J.A. (1999) Optimal interferometer designs for optical coherence tomography. *Optics Letters*, 24, 1484-1486. doi:10.1364/OL.24.001484

[7] Podoleanu, A.Gh. (2000) Unbalanced versus balanced ope- ration in an optical coherence tomography system. *Applied Optics*, **39**, 173-182. doi:10.1364/AO.39.000173

[8] Jang, I.K., Bouma, B.E., Kang, D.H., Park, S.J., Park, S.W., Seung, K.B., Choi, K.B., Shishkov, M., K. Schlendorf, Pomerantsev, E., Houser, S.L., Aretz, H.T. and Tearney, G.J. (2002) Visualization of coronary atherosclerotic plaques in patients using optical coherence tomography: Comparison with intravascular ultrasound. *Journal of the American College of Cardiology*, **39**, 604-609. doi:10.1016/S0735-1097(01)01799-5

[9] Stamper, D., Weissman, N. and Brezinski, M. (2006) Plaque characterization with optical coherence tomography. *Journal of the American College of Cardiology*, **47**, 69-79. doi:10.1016/j.jacc.2005.10.067

[10] Luz, A., Bisceglia, T., Hughes, C., Tammam, K., Farah, B. and Fajadet, J. (2010) Atherosclerotic plaque prolapse between coronary stent struts visualized by optical coherence tomography. *Revista Portuguesa de Cardiologia*, **29**, 143-146.

[11] Patel, N.A., Stamper, D.L. and Brezinski, M.E. (2005) Review of the ability of optical coherence tomography to characterize plaque, including a comparison with intravascular ultrasound. *Cardiovascular and Interventional Radiology*, **28**, 1-9. doi:10.1007/s00270-003-0021-1

[12] Andersen, P.E., Bjarklev, A. and Tycho, A. (2005) Optical amplification in coherent optical frequency modulated continuous wave reflectometry. US Patent No. 6900-943 B2.

[13] Rao, B., Zhang, J., Wang, Q. and Chen, Z. (2007) Investigation of coherent amplification with a semiconductor optical amplifier employed in a swept source OCT system. *Proceedings of SPIE*, **6429**, 642924-1. doi:10.1117/12.704844

[14] Jayavel, P., Amano, T., Choi, D., Furukawa, H., Hiro-Oka, H., Asaka, K. and Ohbayashi, K. (2006) Improved sensitivity of optical frequency domain reflectometry-optical coherence tomography using a semiconductor optical am- plifier. *Japanese Journal of Applied Physics*, **45**, L1317- L1319. doi:10.1143/JJAP.45.L1317

[15] Mao, Y., Chang, S. and Flueraru, C. (2010) Fiber lenses for ultra-small probes used in optical coherent tomography. *Journal of Biomedical Science and Engineering*, **3**, 27-34.

[16] Shiomi, M., Ito, T., Yamada, S., Kawashima, S. and Fan, J. (2003) Development of an animal model for spontaneous myocardial infarction (WHHL-MI rabbit). *Arteriosclerosis*, *Thrombosis*, *and Vascular Biology*, **23**, 1239-1244. doi:10.1161/01.ATV.0000075947.28567.50

[17] Sainter, A.W. King, T.A. and Dickinson, M.R. (2002) Theoretical comparison of light sources for use in optical coherence tomography. *Proceedings of SPIE*, **4619**, 289-299. doi:10.1117/12.491307

[18] Yun, S.H., Boudoux, C., Tearney, G.J. and Bouma, B.E. (2003) High-speed wavelength-swept semiconductor laser with a polygon-scaner-based wavelength filter. *Optics Letters*, **28**, 1981-1983. doi:10.1364/OL.28.001981

[19] Zhu, X., Liang, Y., Mao, Y., Jia, Y., Liu, Y. and Mu, G. (2008) Analyses and calculations of noise in optical coherence tomography systems. *Frontiers of Optoelectronics in China*, **1**, 247-257. doi:10.1007/s12200-008-0034-0

[20] Rosa C. C. and Podoleanu, A. Gh. (2004) Limitation of the achievable signal-to-noise ratio in optical coherence tomography due to mismatch of the balanced receiver, *Applied Optics*, **43**, 4802-4815. doi:10.1364/AO.43.004802

Copyright © 2011 SciRes.